E-ISSN: 2948-5231

Article

Journal of Asian Geography, 2026, Volume 5 (Issue 2), 46-58
https://doi.org/10.36777/jag2026.5.2.5

Comparative Google Earth Engine Workflows for Flood and Landslide Diagnostics in Lower Silesia, Poland, and Batang Kali, Malaysia

Natalia Zaręba[1], Putri Zafira Bianca Putri [2], Mateusz Banasiak [3], Mohd Rahimi Abdul Karim [2], Jakub Stanoszek [3], Zairil Anuar Zulmuji [2], Krzysztof Marian Tomiczek [4,*], Nur Suhaili Mansor [5], Aneta Grodzicka [6]

[1] Surveying and Cartography, Faculty of Mining, Safety Engineering and Industrial Automation, Silesian University of Technology, 2A Akademicka Street, PL-44-100 Gliwice, Poland, EU, MSc Stud.
[2] Master of Science in Geoinformatics for Disaster Risk Reduction, School of Computing, Universiti Utara Malaysia, 06010 UUM Sintok, Kedah Darul Aman, Malaysia, MSc Stud.
[3] Geoinformatics, Institute of Physics, Silesian University of Technology, 2A Akademicka Street, PL-44-100 Gliwice, Poland, EU, MSc Stud.
[4] Department of Geoengineering and Raw Materials Extraction, Faculty of Mining, Safety Engineering and Industrial Automation, Silesian University of Technology, 2A Akademicka Street, PL-44-100 Gliwice, Poland, EU, PhD, Assist. Prof. at SUT,
[5] School of Computing, Universiti Utara Malaysia (UUM, Malaysia), 06010 UUM Sintok, Kedah Darul Aman, Malaysia, PhD, Sen. Lect.,
[6] Department of Geoengineering and Raw Materials Extraction, Faculty of Mining, Safety Engineering and Industrial Automation, Silesian University of Technology, 2A Akademicka Street, PL-44-100 Gliwice, Poland, EU, DSc Prof. at SUT

*Correspondence: Krzysztof.Tomiczek@polsl.pl

Received: 1 Jul 2026; Revised: 15 Sep 2026; Accepted: 27 Sep 2026; Published 29 Sep 2026

Abstract: This study evaluates Google Earth Engine (GEE) as the central computational environment for a unified, repeatable workflow for post-event geospatial diagnostics of two contrasting natural hazards: the September 2024 flood in Lower Silesia, Poland, and the December 2022 Batang Kali landslide in Selangor, Malaysia. Both cases followed the same analytical sequence: pre-event and post-event image selection, generation of a continuous change layer, threshold-based binary mask extraction, z-score standardization of change magnitude, point-based validation, and cartographic export. The flood branch used Sentinel-2 Level-2A imagery and ΔNDWI, whereas the landslide branch used Sentinel-1 GRD SAR imagery and $\Delta\sigma^0$. For the Lower Silesia AOI, the workflow delineated 70.142 km² of flood-class pixels and produced complete agreement for the 240-point internal reference sample. Because the reference points were selected within the classified domain and interpreted from satellite imagery, this 100% agreement is treated as case-specific and potentially optimistic rather than as independent proof of error-free classification. For Batang Kali, all 11 reference landslide points were detected, giving 100% producer's accuracy, but 109 stable reference points were also classified as landslide-like; overall accuracy and user's accuracy were 9.17%. The landslide output is therefore interpreted as a high-sensitivity disturbance-screening product rather than a precise landslide inventory. The results show that GEE provides a transferable computational architecture, while diagnostic performance remains hazard- and indicator-specific.

Keywords: Google Earth Engine; Batang Kali; landslide detection; flood diagnostics; Disaster Risk Reduction

1.0 Introduction

1.1 Scientific Context

The assessment of natural hazards essentially involves obtaining reliable spatial data under operational constraints. Immediately after a flood or landslide, access to the area is often difficult due to damaged infrastructure, unstable terrain, ongoing rainfall, or safety restrictions. At the same time, decision-makers and specialized services need information on the location, extent, and intensity of the event.
Under such conditions, post-event analysis must rely on methods that allow for the transformation of large amounts of remote sensing data into interpretable geographic data-information. Remote sensing, change detection, and GIS are not merely visualization tools but fundamental analytical instruments for disaster assessment (Figure 1). Their research value lies in their ability to capture spatial heterogeneity while preserving the geographic context. They support consistent interpretation across areas differing in land cover, morphology, and hydrometeorological factors.

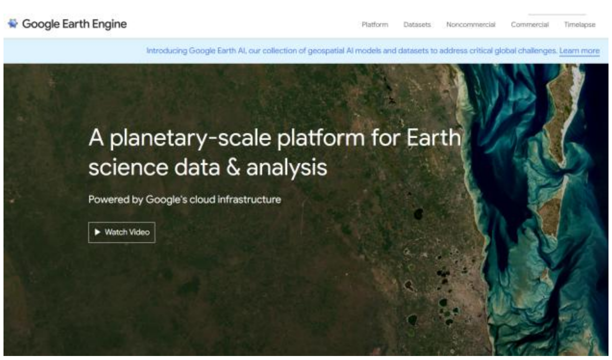

(a)

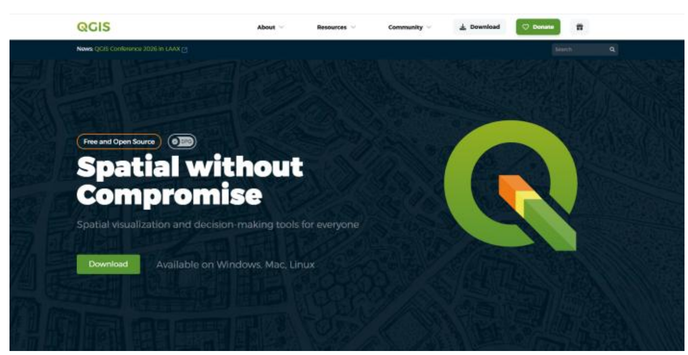

(b)

Figure 1: Google Earth Engine (a) and QGIS (b) platforms (Google Earth Engine; QGIS.org, 2026).

Within this analytical framework, the detection of multi-temporal changes is particularly important because it transforms two measurements of the same area into a concrete measure of surface disturbances. In the case of optical imagery, post-event changes can be expressed using spectral indices that respond to the spread of water, loss of vegetation, or exposure of sediments. For radar images, changes can be captured through differences in backscatter intensity, which reflect changes in roughness, moisture, and vegetation structure (Figure 2).

A key research issue is that the observed 'signal' is never interpreted in isolation. It is interpreted as a geographically organized response to a documented event and within the physical constraints of the analyzed landscape. A rigorous post-event process must combine sensor-specific interpretation with explicit spatial processing, validation, and cartographic synthesis. For floods, water-sensitive optical indices,

E-ISSN: 2948-5231
Article
Journal of Asian Geography, 2026, Volume 5 (Issue 2), 46-58
https://doi.org/10.36777/jag2026.5.2.5

such as the Normalized Difference Water Index (*NDWI*), are often preferred. For landslides, radar-based approaches are particularly attractive because they operate even under cloudy conditions and can detect disturbances where optical observation is limited.

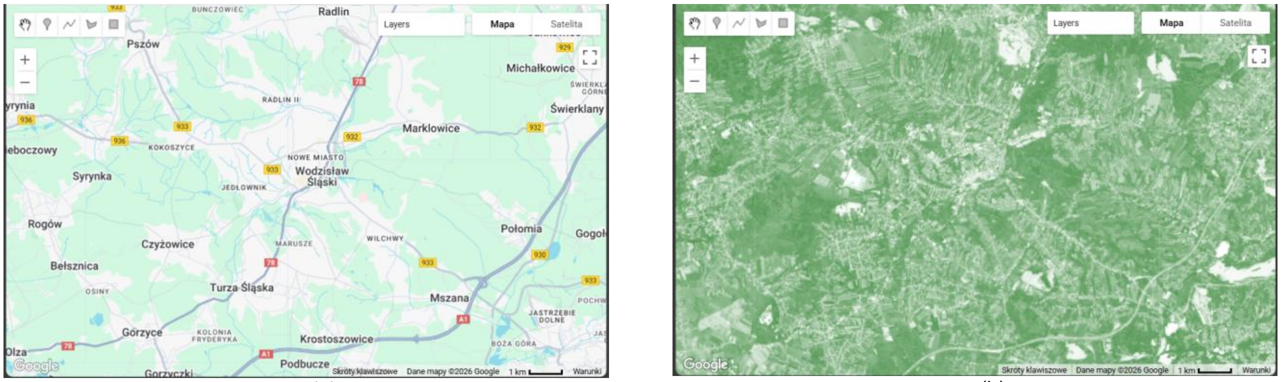

(a) (b)

Figure 2: Auxiliary Polish workflow test area in Wodzisław Śląski, Silesian Voivodeship: location view (a) and an example AOI mask (b). These panels illustrate workflow development and are not part of the quantitative Lower Silesia AOI. (Google; QGIS.org, 2026, 2026).

1.2 *Google Earth Engine as a Central Analytical Environment*

Google Earth Engine should be viewed as a computational architecture that makes it technically feasible to compare two different hazards. Google Earth Engine (GEE) provides direct access to an extensive, curated archive of satellite and geospatial datasets, including Sentinel-1 and Sentinel-2 data. There is no need to download and store all raw imagery locally. GEE provides large-scale cloud computing capabilities, allowing the same analytical logic to be applied efficiently across different study areas and to different types of measurements

A key advantage of GEE is its support for reproducible scripts. Every processing step, from image filtering to thresholding and data export, can be documented, rerun, and modified. Derived rasters, tables, and other outputs can be exported for subsequent validation and cartographic refinement. GEE provides a common environment in which workflows for optical and radar data can be designed using a unified processing logic while preserving their distinct physical interpretations. These features are central to the platform, as described in the official documentation and in the seminal Earth Engine paper by Gorelick et al. (2017).

In this analysis, this shared computational environment is of particular methodological importance.

The 2024 flood in Lower Silesia, Poland, and the 2022 landslide in Batang Kali, Malaysia, differ in terms of process mechanics, environmental conditions, and sensor responses. However, both phenomena can be analysed using the same Earth Engine workflow:

- selection of pre- and post-event images;
- determination of pixel-level changes;
- generation of threshold-based masks;
- calculation of regional statistics; and
- export of hazard layers for comparison with reference information.

Earth Engine thus enables a controlled comparison between the two hazards. The flood analysis is based on the optical response to the expansion of surface water, expressed as ΔNDWI, whereas the landslide analysis is based on the radar response to post-event surface disturbances, expressed as $\Delta\sigma^{o}$. The comparative strength of the study therefore depends on the use of a single, consistent cloud-based analytical system for both hazards.

1.3 *Objectives of the Study*

Flood and landslide mapping have both been widely studied using remote sensing and GEE, but most published applications remain hazard-specific or sensor-specific. The gap addressed here is narrower: relatively few studies use a single, coherent GEE processing logic to compare two physically different hazards while preserving the distinct interpretations of optical and radar change signals (DeVries et al., 2020; Nghia et al., 2022; Phakdimek et al., 2023; Singh & Rawat, 2024; Yang et al., 2024).

The principal contribution of this study is methodological. It tests the transferability of a single cloud-based processing architecture across two hazard types rather than proposing a universal physical indicator. Its secondary contribution is operational, as the workflow relies on freely available Sentinel data, reproducible scripts, and open-source GIS tools that can support rapid post-event screening and teaching-oriented replication.

The workflow differs from single-hazard GEE applications by keeping the computational sequence consistent while changing the physically appropriate observable: ΔNDWI for flood-related surface-water expansion and $\Delta\sigma^{o}$ for radar-detected slope disturbance. This design allows workflow transferability to be evaluated separately from classification performance and highlights where hazard-specific refinement is required (DeVries et al., 2020; Handwerger et al., 2022; Mullissa et al., 2021; Nghia et al., 2022; Phakdimek et al., 2023; Santangelo et al., 2022; Singh & Rawat, 2024; Yang et al., 2024).

The analysis had three interrelated objectives:

1. To evaluate a Google Earth Engine-based optical workflow for detecting and characterising the September 2024 flood in Lower Silesia using Sentinel-2 imagery and the ΔNDWI change index.
2. To evaluate a Google Earth Engine-based radar workflow for detecting and characterising landslides in Batang Kali using Sentinel-1 imagery and the $\Delta\sigma^{o}$ backscatter change index.
3. To compare the interpretive value, analytical strengths, and uncertainty structures of the two workflows within a common, standardised change-intensity framework.

Neither case is treated as a benchmark for the other. Each represents an empirical test of the same computational architecture under different physical conditions, geographic settings, and sensor constraints. The comparison is therefore methodological rather than a claim of geographic or process equivalence.

E-ISSN: 2948-5231
Article Journal of Asian Geography, 2026, Volume 5 (Issue 2), 46-58
https://doi.org/10.36777/jag2026.5.2.5

2.0 Study Areas

2.1 Batang Kali, Selangor, Malaysia

Batang Kali is located in the Hulu Selangor district, in the northeastern part of the state of Selangor on the Malay Peninsula. Geographically, the region serves as a transitional zone between the more densely populated valleys and roadside areas and the steeper upland terrain characteristic of the district's mountainous interior. Hulu Selangor covers a large area with varied topography. Its main settlement areas include Batang Kali, Serendah, and Kuala Kubu Bharu. The district is characterised by diverse terrain, numerous river basins, and strong interactions among forested and agricultural areas, transportation corridors, and expanding urban areas.

These conditions are significant for landslide analysis because the case combines steep slopes, exposure to heavy rainfall, and increasing human presence within a region that is not geotechnically uniform. From a geomorphological and geotechnical perspective, the Batang Kali area is susceptible to rainfall-triggered landslides. Studies of areas such as Hulu Selangor indicate that slope gradient, land use, rainfall, proximity to rivers, and proximity to roads are important factors influencing local landslide susceptibility.

This is consistent with the region's overall physical structure, where fragmented slopes, converging drainage systems, and linear infrastructure create recurring conditions conducive to hydrologically induced slope instability. The area is also strongly influenced by natural drainage systems, including the Sungai Selangor watershed, and its topography reflects close interactions among runoff concentration, vegetation cover, and local terrain.

Intense or cumulative rainfall can increase pore-water pressure and reduce effective stress in susceptible slope materials, particularly where steep slopes, concentrated drainage, weathered materials, and surface disturbance act together. Recent susceptibility analysis for Hulu Selangor likewise identifies slope, lithology, proximity to rivers, proximity to roads, land use, and rainfall as relevant conditioning factors (Ibrahim et al., 2025).

Land cover and land use further highlight the importance of the Batang Kali region for natural hazard research. The Hulu Selangor area remains predominantly forested, with forested areas accounting for 51.7% of the district's total land area and agricultural areas accounting for 35.7%. Smaller but spatially significant areas are occupied by residential, transportation, infrastructure, and other built-up areas (Majlis Perbandaran Hulu Selangor, 2023).

This mosaic is important for interpreting remote sensing data. Forested areas can mask subtle pre-disaster changes in optical imagery, while mixed vegetation, cleared areas, and infrastructure edges can affect radar backscatter following a disaster. Batang Kali is also not an isolated mountainous area. It lies within a region where building density, transportation networks, and recreational land use have expanded and continue to expand, increasing the number of vulnerable elements near potentially unstable slopes. This makes the area particularly relevant for geospatial hazard assessment.

The landslide disaster of December 2022 underscored this threat in a particularly tragic way. The incident occurred on 16 December 2022 at a campsite near Batang Kali in Hulu Selangor. According to the official report, 92 people were involved in the incident, of whom 61 were rescued and 31 lost their lives. The report stated that the landslide was primarily a natural slope failure influenced by rainfall and geological conditions. Reports based on declassified investigation findings indicate that it had rained for five consecutive days before the incident, with 118.6 mm of rainfall recorded during that period. A total of 444.8 mm had fallen over the preceding 30 days. These figures are consistent with the interpretation of the event as a rainfall-induced landslide in a tropical mountainous environment already susceptible to landslides (Associated Press, 2023).

Batang Kali therefore provides a relevant tropical mountain case for testing Sentinel-1 and GEE as rapid post-event tools for detecting radar-observed surface disturbances. The case is particularly relevant to Malaysia and tropical Asia because dense vegetation, frequent cloud cover, intense monsoon rainfall, and complex terrain can constrain rapid optical assessment and complicate the interpretation of SAR change signals (Phakdimek et al., 2023; Santangelo et al., 2022; Yang et al., 2024).

2.2 Lower Silesia, Poland

Lower Silesia is an important region in southwestern Poland, located within the temperate climate zone of Central Europe and traversed by the Oder River and its network of tributaries. In terms of physiography, the region comprises extensive lowland and foothill areas, together with higher-elevation terrain in the south associated with the Sudeten Mountains. This topographic contrast is significant for flood analysis. Runoff from the southern and border areas, which receive relatively high precipitation, can be conveyed towards river corridors with gentler gradients and inhabited floodplains further north and northeast.

In regional development documents, the Oder is described as the main river flowing through the Lower Silesian Voivodeship. The southern mountainous areas are identified as among the coldest and wettest parts of the region, whereas the lowland zone occupies a substantial proportion of the province. This combination of mountainous headwater areas and downstream lowland floodplains represents an important hydrological characteristic of Lower Silesia.

The land-use structure of Lower Silesia also provides a suitable context for a flood case study (Figure 3). The region contains a substantial proportion of agricultural land, extensive lowland areas, well-developed transportation corridors, and urbanised areas, particularly within the broad Oder River valley. Regional data indicate that agricultural land accounts for 52.8% of the Lower Silesian Voivodeship, while forests and other wooded areas account for 29.4%. This landscape creates a diverse floodplain environment in which a single flood event can affect open areas, waterways, industrial infrastructure, settlements, and transportation networks.

From a geospatial flood-mapping perspective, this diversity is useful because optical imagery can capture strong contrasts between newly inundated areas, stable non-inundated surfaces, and adjacent built-up zones. It also provides suitable conditions for point-based post-event validation, as flooded and non-flooded reference points can be sampled across different land-cover contexts rather than being restricted to a single homogeneous valley floor.

The floods in September 2024 subjected the region to severe hydrometeorological stress. Between 13 and 16 September 2024, Storm Boris brought exceptionally heavy rainfall to parts of Central Europe and caused severe flooding in southwestern Poland. European reports and emergency agencies identified Lower Silesia as one of the most severely affected regions in Poland. Copernicus and ECMWF summaries describe the event as one of the major flood events in Europe in 2024. Field reports also documented severe impacts across southwestern provinces, including Lower Silesia. This large-scale flood therefore provides an appropriate regional context for a targeted geospatial case study based on post-event water detection. Within this regional setting, the study area of interest (AOI) covers the flood-affected lowland corridor of Lower Silesia. Using Sentinel-2 data, changes in surface-water extent can be assessed across river channels, floodplain areas, and adjacent built-up zones.

E-ISSN: 2948-5231
Article
Journal of Asian Geography, 2026, Volume 5 (Issue 2), 46-58
https://doi.org/10.36777/jag2026.5.2.5

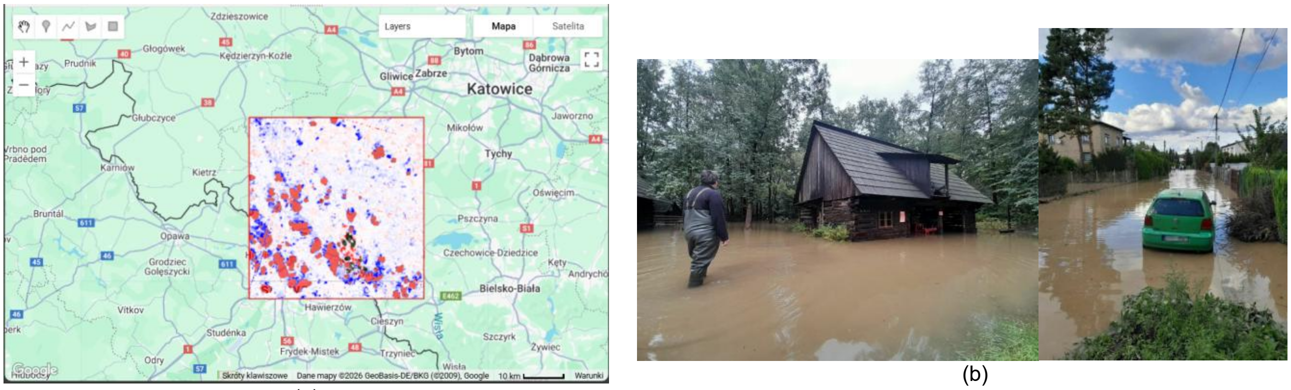
(a) (b)

Figure 3: Auxiliary Wodzisław Śląski test area in the Silesian Voivodeship (a), showing the flood-related classes used during workflow development, and field photographs illustrating the 2024 flood context (b). (Source: Nasze Miasto, 2024)

The project used several demonstration locations in Poland during workflow development. Wodzisław Śląski, located in the Silesian Voivodeship rather than Lower Silesia, served as an auxiliary test location (Figure 4). The quantitative flood results reported in this article refer exclusively to the Lower Silesia AOI defined in Section 3.3.1. The common workflow included ΔNDWI calculation, binary flood-mask generation, standardised change mapping, and point-based validation.

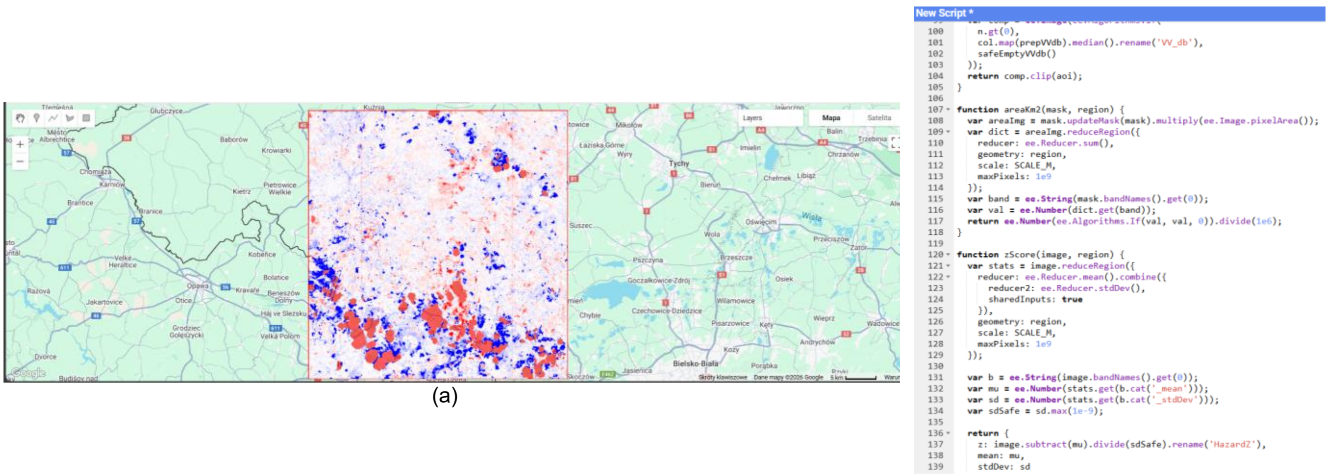

(a) (b)

Figure 4: Auxiliary Wodzisław Śląski workflow test area (a) and an excerpt from the GEE script used during method development (b).

The Lower Silesia validation dataset contains 240 points, distributed equally between the two predicted classes. Candidate points were generated through stratified sampling of the classified output, and reference labels were assigned through manual visual interpretation using Copernicus Browser and NASA Worldview imagery, as documented in the project workflow (Tomiczek, 2026). Because the reference interpretation relied on satellite imagery rather than an independent field-based inventory, the validation is considered an internal, image-based assessment (Copernicus Data Space Ecosystem; NASA, 2026).

2.3 Justification of the Analyses from a Geographical Perspective

The issues examined in this article are not based on geographical similarities. Batang Kali and Lower Silesia differ fundamentally in terms of climate, terrain, dominant physical processes, and sensor responses. However, the comparison is justified by their methodological equivalence. Both areas:

- represent actual post-disaster settings;
- were analysed using Google Earth Engine;
- were processed according to a common analytical logic involving pre- and post-event comparison, derivation of change layers, calculation of standardised change intensity, and point-based validation.

They therefore provide a controlled basis for comparing two satellite sensor systems, two physically distinct change indicators, and two different manifestations of natural hazards within a single, repeatable geospatial framework.

3.0 Data, Materials and Methodology

3.1 General Research Design

The analysis was implemented in Google Earth Engine for two distinct disaster types: the September 2024 flood in Lower Silesia, analysed using Sentinel-2 optical imagery, and the rainfall-induced landslide in Batang Kali, analysed using Sentinel-1 SAR imagery.

In both cases, the workflow followed the same six-step logic:

Journal of Asian Geography, 2026, Volume 5 (Issue 2), 46-58
https://doi.org/10.36777/jag2026.5.2.5
E-ISSN: 2948-5231

- selection of pre- and post-event imagery;
- calculation of a case-specific change index;
- extraction of a binary event mask;
- standardisation of continuous change values into a dimensionless change-intensity layer;
- validation using reference points and error matrices; and
- preparation of final cartographic outputs for interpretation and comparison.

This structure maintained methodological equivalence while allowing the physical meaning of the derived indicators to remain specific to each hazard. The overall analysis follows the script-based geospatial analysis framework implemented in Google Earth Engine (Gorelick et al., 2017).

3.2 Theoretical Foundations

3.2.1 Change Detection Using Remote Sensing as an Analytical Principle

The analytical basis of the study was change detection in a multi-temporal context. In its most general form, change detection relies on comparing two observations of the same area obtained at different times, and its goal is to determine the scale and spatial distribution of disturbances resulting from an event. According to Singh, the underlying logic is not merely a visual comparison, but the pixel-level transformation of two images from different periods into a distinct difference image, which then becomes the primary subject of interpretation. In this study, the general equation for change is introduced as:

$$\Delta I(x,y)=I_{post}(x,y)-I_{pre}(x,y) \tag{1}$$

where:

$I_{pre}(x,y)$ and $I_{post}(x,y)$ represent the values of the selected indicator before and after the event at pixel (x,y).

This equation is intentionally sensor neutral. It can express a change in a spectral index for the flood case and a change in radar backscatter for the landslide case. Its utility lies in suppressing stable background conditions and emphasizing spatially organized post-event change.

A key methodological implication is that the physical meaning of ΔI depend on the observation area. A positive change in the water-sensitive optical index is not physically equivalent to a negative change in SAR backscatter, even though both indicate disturbance. For this reason, the analytical framework employed does not assume a single universal index. Instead, it assumes a single universal analytical logic and two physically distinct observables of diagnostic significance. This distinction maintains equivalence at the workflow level while preventing false equivalence at the data interpretation level.

3.2.2 Physical Basis of the NDWI and ΔNDWI Indices

In the case of flooding, the primary observable quantity is the Normalized Difference Water Index (*NDWI*). McFeeters defined the NDWI as a normalized spectral transformation using reflectance in the green and near-infrared bands. It enhances open water features while suppressing vegetation and soil. Equation:

$$NDWI = \frac{G - NIR}{G + NIR} \tag{2}$$

where:

G - denotes the albedo in the green band,

NIR - denotes the albedo in the near-infrared band.

In Sentinel-2 Level 2A data, these correspond to band B3 and band B8, respectively. Open water typically exhibits a relatively low reflectance in the near-infrared band and a stronger contrast relative to the green band. The *NDWI* value tends to increase in areas where a pixel covers a water surface.

The analysis did not use the *NDWI* index itself, but rather the temporal difference in *NDWI* before and after the flood:

$$\Delta NDWI=NDWI_{post}-NDWI_{pre} \tag{3}$$

A positive $\Delta NDWI$ value indicates an increased presence of water after the event and therefore serves as a practical indicator of increased flooding or surface wetting associated with the flood.

However, $\Delta NDWI$ remains an interpretive simplification. It is sensitive not only to open water. Cloud contamination, residual atmospheric effects, mixed pixels at water land boundaries, and changes in surface moisture or vegetation cover can cause interference. For this reason, $\Delta NDWI$ is best treated as a physically interpretable but threshold-dependent flood indicator, rather than as a direct hydrodynamic measurement.

3.2.3 Physical Principles of Sentinel-1 Backscatter and $\Delta\sigma^0$

For landslides, the primary observable is the change in radar backscatter derived from Sentinel-1 C-band SAR data. The official observation documentation and Earth Engine define Sentinel-1 GRD as a radar product. It operates in all weather conditions, day and night, is corrected for terrain, and is suitable for analyzing surface changes. In such data, the backscatter coefficient σ^0 reflects the interaction of the emitted radar wave with the observed surface. Its magnitude depends on roughness on the radar wavelength scale, dielectric properties (which are strongly influenced by moisture), vegetation structure, and acquisition geometry, including the local orientation of the slope relative to the line of sight.

Changes caused by a landslide:

$$\Delta\sigma^0=\sigma^0_{post}-\sigma^0_{pre} \tag{4}$$

In many situations following a landslide, strongly negative values $\Delta\sigma^0$ indicate a decrease in radar backscatter, which may be associated with vegetation removal, surface smoothing or denudation, or other forms of abrupt slope disturbance.

This is the interpretation applied in the Batang Kali case. Strongly negative $\Delta\sigma^0$ values were treated as landslide-like surface-disturbance candidates and were converted into a binary screening mask and a standardized disturbance-intensity layer. They were not assumed to constitute a landslide inventory without validation.

At the same time, the significance of negative values $\Delta\sigma^0$ is not always clear-cut.

Recent studies of landslides using SAR data show that post-event changes in reflectivity can vary depending on land cover, landslide type, slope aspect, roughness transformation, and soil moisture conditions. In practice, this means that radar anomaly changes can be highly sensitive to the occurrence of landslides. At the same time, the anomaly may generate false alarms in areas where disturbances are

E-ISSN: 2948-5231
Journal of Asian Geography, 2026, Volume 5 (Issue 2), 46-58
https://doi.org/10.36777/jag2026.5.2.5

geomorphologically likely but cannot be directly attributed to a specific landslide. This uncertainty is an expected consequence of interpreting a complex microwave signal over steep and heterogeneous terrain.

3.2.4 Binary Processing, Mask Generation, and Uncertainty

Thresholding converts a continuous change field into a binary screening product. In the flood case, pixels were classified as flood-like when Δ*NDWI* exceeded a positive threshold; the archived workflow used ΔNDWI ≥ 0.25. In Batang Kali, pixels were classified as landslide-like when the smoothed $\Delta\sigma^0$ was equal to or below a negative threshold, with the project workflow allowing either a fixed value or an adaptive percentile-based threshold. Threshold choice controls the balance between sensitivity and commission error. A more permissive threshold generally increases detection sensitivity but also increases false positives, whereas a stricter threshold may improve precision at the cost of additional false negatives. The threshold values used here originated from the exploratory PBL workflow rather than from an independently optimized calibration set. (Tomiczek, 2026)

The archived project outputs do not preserve a complete threshold-sensitivity sweep for either case. A retrospective sensitivity curve therefore cannot be reported without rerunning the original analyses. This limitation is stated explicitly and should be addressed in future applications by testing multiple thresholds against an independent reference dataset. (Foody, 2002; Singh, 1989)

Z-score Standardization and Accuracy Assessment

Because Δ*NDWI* and $\Delta\sigma^0$ have different physical units and response directions, the z-score is used only to express the relative extremeness of change within each AOI. It does not represent a validated physical measure of hazard intensity. For a change variable I, the standardized value is $Z = (I - \mu) / \sigma$, where μ and σ are the AOI mean and standard deviation, respectively. Positive or negative Z values retain the direction of the original change variable. Accordingly, the resulting layers are referred to here as standardized change intensity for the flood case and standardized disturbance intensity for the landslide case.

Classification agreement was summarized from true positives (TP), true negatives (TN), false positives (FP), and false negatives (FN). The reported measures were OA = (TP + TN)/(TP + TN + FP + FN), user's accuracy/precision = TP/(TP + FP), producer's accuracy/recall = TP/(TP + FN), specificity = TN/(TN + FP), F1 = 2TP/(2TP + FP + FN), and balanced accuracy = 0.5. (Foody, 2002)

3.3 Data Sources

3.3.1 The Flood in Lower Silesia

The Lower Silesia flood analysis used the COPERNICUS/S2_SR_HARMONIZED Sentinel-2 Level-2A surface-reflectance collection in GEE. *NDWI* was calculated from B3 (green) and B8 (near infrared), both at 10 m native pixel size. The archived script used the QA60 bit mask to remove opaque cloud and cirrus pixels and then produced median pre-event and post-event composites. Google documents QA60 bits 10 and 11 as the opaque-cloud and cirrus flags and notes that legacy-consistent QA60 information is available for 2024 scenes.(European Space Agency; Google for Developers, 2026)

The Lower Silesia AOI was defined by 16.85-17.45° E and 50.85-51.25° N. The pre-event window was September 1-10, 2024 (four usable scenes), and the post-event window was September 16-25, 2024 (three usable scenes). B2, B3, B4, B8, and QA60 were retained in the project stack. The Δ*NDWI* analysis was performed at the native 10 m scale of B3 and B8. A separate scene-level CLOUDY_PIXEL_PERCENTAGE criterion and an additional raster-resampling step are not documented in the archived final workflow and are therefore not reported as if they had been applied. (European Space Agency; Google for Developers, 2026)

3.3.2 The Batang Kali Landslide Case

The Batang Kali analysis used the COPERNICUS/S1_GRD collection in GEE. The archived project workflow specifies C-band Sentinel-1 GRD data, VV polarization, and Interferometric Wide Swath (IW) mode. The Earth Engine collection is radiometrically calibrated, terrain corrected, and provided in decibels; the catalog documents thermal-noise removal, radiometric calibration, and terrain correction as standard preprocessing steps.(Google for Developers, 2026; Mullissa et al., 2021) The project materials describe approximately 10 m ground sampling for the selected high-resolution GRD products.

Pre-event and post-event Sentinel-1 composites were compared through $\Delta\sigma^0$, followed by spatial smoothing before thresholding. The archived manuscript and project presentation do not retain the exact Sentinel-1 product identifiers, acquisition dates, orbit direction, relative-orbit number, or smoothing-kernel size. These parameters are therefore not reconstructed by assumption. Their absence limits full scene-level reproducibility and should be corrected from the original GEE project history before final resubmission if those records remain available. (Google for Developers, 2026; Mullissa et al., 2021)

3.4 Google Earth Engine Analytical Architecture

Google Earth Engine is the environment in which the entire computational workflow was implemented. In both case studies, the image datasets were filtered based on the geometry of the area of interest (AOI) and the pre- and post- event time periods.

For the flood case, cloud and cirrus pixels were removed with the QA60 mask before median compositing. For the landslide case, Sentinel-1 GRD scenes were filtered by AOI, time, VV polarization, and IW mode, and the resulting backscatter change layer was spatially smoothed before thresholding. GEE does not apply application-specific speckle filtering automatically; such filtering must be implemented explicitly, which is why the smoothing operation is reported separately here. (Google for Developers, 2026; Mullissa et al., 2021)

The two workflows differed primarily in terms of physical observables, rather than computational logic. The Earth Engine scripting model and GEE server-side processing make such a (parallel) project technically efficient and methodologically transparent (Figure 5).

The second element was the pixel-level transformation of pre- event and post-event composites into continuous change layers. For Lower Silesia, this involved calculating the *NDWI* index based on surface reflectance, followed by deriving Δ*NDWI*.

The third component involves regional statistics, threshold determination, and raster data export. Earth Engine was used to calculate the mean and standard deviation at the Area of Interest (AOI) level. Earth Engine was also used to apply binary classification rules and to calculate area statistics for the detected hazard class (Figure 5). The analysis process for Lower Silesia generated the mean and standard deviation at the area of interest level Δ*NDWI* along with a flood area estimate, and the process for Batang Kali used the same logic.

Finally, the derived rasters were exported as GeoTIFF files for external validation, map creation, and reporting in QGIS.

This architecture combines access to archives, large-scale server-side computations, repeatable scripts, and interoperability with external GIS software. In practice, Earth Engine enables the execution of equivalent processes in two very different hazard environments without fragmenting the computing environment.

E-ISSN: 2948-5231
Article
Journal of Asian Geography, 2026, Volume 5 (Issue 2), 46-58
https://doi.org/10.36777/jag2026.5.2.5


(a)

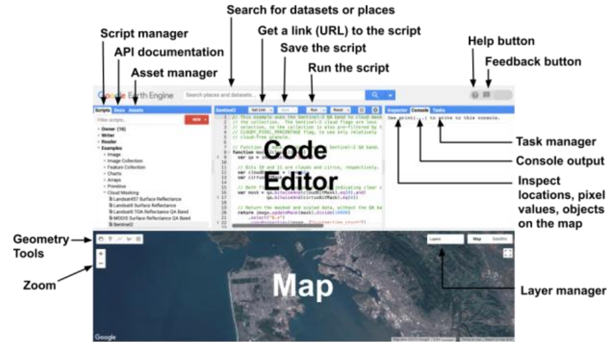

(b)

Figure 5: A view of the landslide in Batang Kali (a) and a diagram of the Google Earth Engine work view (b).

The binary flood mask used $\Delta NDWI \geq 0.25$. The continuous $\Delta NDWI$ field was then standardized with the AOI mean (0.0014716383) and standard deviation (0.1463424363) to produce a dimensionless standardized change-intensity layer. The thresholded flood-class area within the AOI was 70.142 km².

The verification was conducted using reference points and a two-class error matrix. A total of 240 samples and a balanced reference structure were included. The final products exported from Earth Engine consisted of at least three analytically distinct results:

- a continuous layer $\Delta NDWI$,
- a binary flood mask,
- a standardized change-intensity grid.

These were then prepared for mapping and layout in QGIS, where map elements such as the legend, scale, and coordinate grid were added.

3.5 Workflow for the Batang Kali Landslide

The workflow for the Batang Kali landslide followed a parallel structure but was implemented using SAR imagery from the Sentinel-1 satellite and a change index tailored to radar data. The area of interest (AOI) covered the documented site of the Batang Kali landslide, and the processing logic involved comparing post-event backscatter behaviour with the pre-event baseline within the spatially confined slope environment. Sentinel-1 was the primary data source. Its ability to observe the Earth through cloud cover during both day and night makes it particularly suitable for monitoring landslides in tropical environments prone to heavy rainfall.

Within Earth Engine, the main task was to derive the change in backscatter relative to the baseline, expressed as $\Delta\sigma^o$, in accordance with Equation (4), as shown in Figure 6. This was a crucial stage of the coding process, as strongly negative $\Delta\sigma^o$ values were interpreted as indicators of potential surface disturbances consistent with landslide activity. Because raw radar-change data are susceptible to speckle and local variability, smoothing was applied as part of the pre-thresholding process.

A binary landslide-like disturbance mask was then generated by classifying pixels for which the smoothed $\Delta\sigma^o$ values were less than or equal to a negative threshold. The threshold can be adaptive, for example, based on percentiles, or fixed as a fallback approach. The continuous $\Delta\sigma^o$ field was standardised using a z-score to express the relative extremeness of radar backscatter change within the AOI. This product is termed a standardised disturbance-intensity layer rather than a hazard-intensity layer because the magnitude of the z-score alone does not quantify landslide probability, susceptibility, or risk. Conceptually, the Batang Kali workflow yielded the same three-level product structure as the flood analysis in Poland:

- a continuous change layer;
- a binary event mask; and
- a standardised intensity layer.

The mapped standardised disturbance values were strongest on parts of the steep hillslope and lower across much of the surrounding terrain. These patterns were subsequently evaluated against reference points rather than interpreted as a validated hazard zonation. Candidate validation points were organised using the same two-class logic as in the flood case, and reference classes were assigned through manual interpretation of available imagery, as documented in the project workflow (Tomiczek, 2026). Because the reference interpretation was image-based and did not rely on an independent, field-verified landslide inventory, the resulting accuracy measures are treated as screening-performance indicators rather than as definitive measures of landslide detection accuracy.

The final methodological step involved raster export and subsequent preparation of cartographic products in a GIS environment. Figure 7 shows the $\Delta\sigma^o$ change raster and binary landslide-like disturbance mask, while Figure 8 shows the standardised disturbance-intensity layer. The Batang Kali case is not methodologically subordinate to the Lower Silesia case; rather, both cases are equivalent in terms of workflow design while retaining hazard-specific physical interpretations

.

4.0 Results

Both case studies were completed using the same GEE-centred processing sequence, producing continuous change layers, threshold-based binary masks, standardised change-intensity layers, validation outputs, and GeoTIFF products. The principal methodological result is therefore the successful application of a common computational workflow across two different hazard types, while classification performance is reported separately for each case.

The same analytical logic was applied to both case studies using Google Earth Engine (Figure 6). The process began with the selection of pre- and post-event scenes, followed by the derivation of a continuous change layer, extraction of a binary event mask, standardisation of relative change using z-scores, point-based validation, and export of raster results for map preparation in QGIS.

E-ISSN: 2948-5231

Article

Journal of Asian Geography, 2026, Volume 5 (Issue 2), 46-58

https://doi.org/10.36777/jag2026.5.2.5

The main contribution is methodological: the computational sequence was reproducible across the two cases, whereas the accuracy and interpretation of the final products remained hazard-specific. The workflow was implemented using freely available Sentinel data, GEE, and QGIS (Figure 6). No claim is made that the same thresholds or classification performance can be transferred directly to other events without recalibration and independent validation.

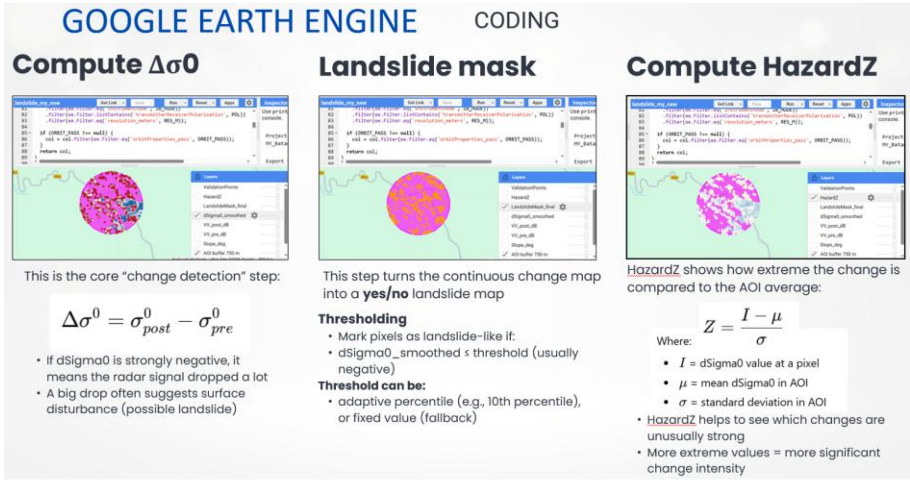

Figure 6: A simplified diagram of the data analysis process in GEE, developed as part of a student research study.

The Batang Kali analysis produced a physically distinct set of outputs based on Sentinel-1 SAR imagery and the $\Delta\sigma^0$ backscatter-change metric. GEE was used to generate the continuous $\Delta\sigma^0$ change layer, a binary landslide-like disturbance mask, a standardized disturbance Z-score layer, and the validation sample. The maps show clusters of strong negative $\Delta\sigma^0$ values on parts of the Batang Kali hillslope. These changes are consistent with abrupt surface disturbance, but the radar response is not unique to landsliding and may also reflect changes in moisture, vegetation, roughness, or viewing geometry.(Mullissa et al., 2021; Phakdimek et al., 2023; Santangelo et al., 2022). The binary mask retained a clustered pattern of landslide-like pixels, while the surrounding AOI contained a mixture of low-change and falsely detected locations. The standardized disturbance layer ranked the magnitude of local change relative to the AOI background; it was not interpreted as a validated hazard-probability surface.

4.1 Batang Kali Landslide Case

An equally comprehensive but physically distinct set of results was developed for Batang Kali, based on Sentinel-1 radar imagery and the $\Delta\sigma^0$ reflectance change index. As part of this process, Google Earth Engine was used to generate a layer of continuous radar changes, convert it into a binary landslide mask, normalise the results to the Hazard Z layer, and compare the results with validation points. The resulting maps show a clear concentration of strong negative backscatter anomalies on steep slopes in the Batang Kali area. These negative values were interpreted as indicators of sudden surface disturbances, (likely) associated with vegetation removal, soil displacement and other forms of landslides.

The two-component landslide mask retained this pattern of concentration. Pixels classified as landslides were grouped in sectors comprising steep and geomorphologically likely slopes. The surrounding areas were dominated by the 'stable' class. The Hazard Z layer added a second level of interpretation by ranking the extremes of variation relative to the background of the area of interest (AOI). High and very high hazard classes were concentrated in the same zones of disturbed slopes. Low-intensity classes dominated on gentler terrain and in valley sectors (macro AOI). This spatial pattern indicates that the analytical process responded to an ordered field of disturbances rather than random variations. The radar product was not arbitrary; it detected a significant pattern of post-event anomalies within the complex environment of tropical slopes.

Strong negative $\Delta\sigma^0$ values indicate a substantial reduction in radar backscatter and were used as the primary disturbance signal in the Batang Kali workflow (Figure 7.a). Moderate negative changes surround parts of the strongest anomalies. Positive or near-zero changes occur elsewhere and can reflect stable surfaces as well as moisture, roughness, or geometric effects unrelated to slope failure.

The landslide-like pixels shown in Figure 7.b are concentrated in parts of the hillslope, but the validation results demonstrate that the binary mask substantially over-detects the target class. The map should therefore be read as a screening mask rather than as a landslide inventory.

Figure 8 shows the standardized disturbance-intensity classes derived from the z-score transformation. Higher classes indicate more extreme radar change relative to the AOI distribution; they do not, by themselves, represent validated levels of landslide hazard or risk.

Table 1 shows the confusion matrix for landslide detection in Batang Kali (2022). The individual labels are:

- True Positive (TP) - locations correctly identified as landslides by the model and confirmed as landslides in the reference data.
- False Positive (FP) - locations identified as landslides by the model but actually stable according to the reference data (over-detection).
- False Negative (FN) - locations classified as stable by the model but actually landslides in the reference data (missed landslides).
- True Negative (TN) - locations correctly classified as stable by both the model and the reference data.

Table 2 shows the accuracy metrics of landslide detection (Batang Kali, 2022).

Article
E-ISSN: 2948-5231
Journal of Asian Geography, 2026, Volume 5 (Issue 2), 46-58
https://doi.org/10.36777/jag2026.5.2.5

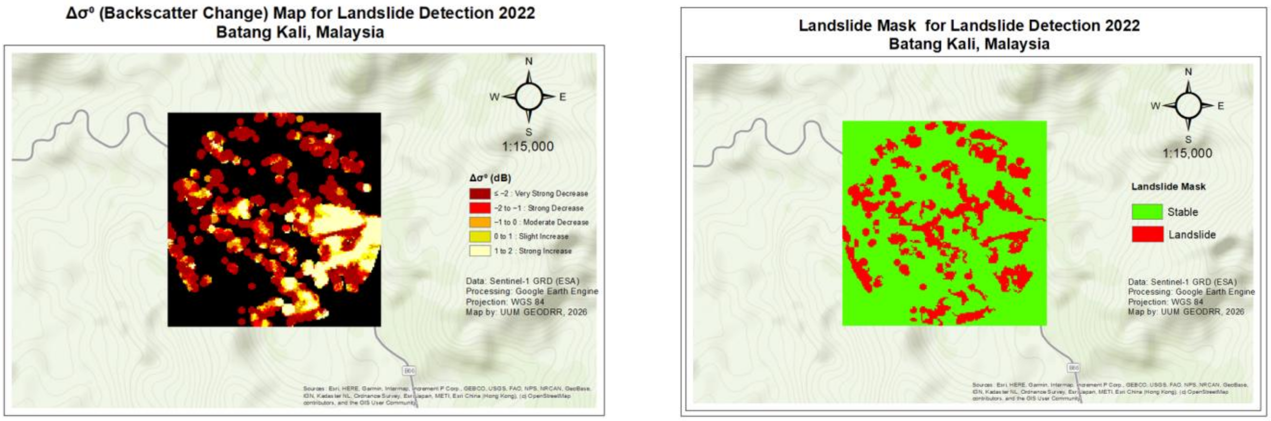

(a) (b)

Figure 7: Sentinel-1 Δσ° backscatter-change map (a) and binary landslide-like disturbance mask (b) for Batang Kali, Malaysia, 2022.

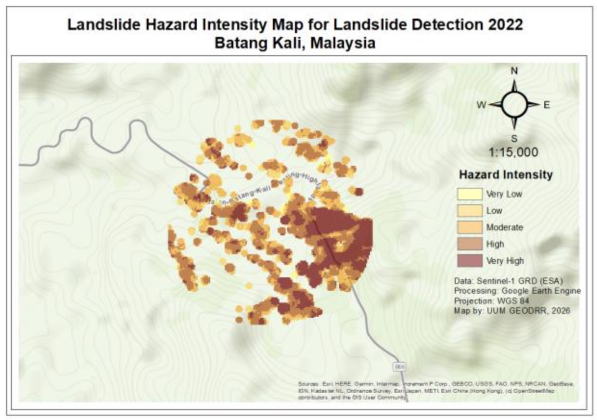

Figure 8: Standardised disturbance-intensity (z-score) map for the 2022 Batang Kali landslide.

Table 1: Confusion matrix for landslide detection in Batang Kali.

Predicted \ Reference	Landslide	Stable	Total
Landslide (1)	11 (TP)	109 (FP)	120
Stable (0)	0 (FN)	0 (TN)	0
Total	11	109	120

Table 2: Accuracy metrics of landslide detection

Metric	Value
Total samples (N)	120
Overall Accuracy (OA)	0.0917 (9.17%)
User's Accuracy - Landslide (UA)	0.0917 (9.17%)
Producer's Accuracy - Landslide (PA)	1
Sensitivity / Recall	1.0000 (100%)
Specificity	0.0000 (0%)
Precision	0.0917 (9.17%)
F1-score	0.1679 (16.79%)
Balanced Accuracy	0.5000 (50%)

The Batang Kali confusion matrix contains 11 TP, 109 FP, 0 FN, and 0 TN (N = 120). The sample therefore contains confirmed reference locations for both landslide and stable classes, but the classifier assigns every sampled location to the landslide-like class. This pattern indicates severe commission error rather than an absence of stable reference points. Overall accuracy and user's accuracy/precision were 9.17%, while producer's accuracy/recall was 100%. The same matrix gives specificity = 0%, F1-score = 16.79%, and balanced accuracy = 50%. These metrics show high sensitivity to the reference landslide points but no discriminatory performance for the stable class.

The Batang Kali binary output is therefore a high-sensitivity disturbance screen with substantial over-detection. It is not a precise landslide inventory and should not be used as a stand-alone susceptibility, hazard, or risk map. The absence of false negatives in this sample is useful for screening, but the 109 false positives show that a simple Δσ° threshold is insufficiently selective for operational mapping in this tropical setting. This behavior is consistent with the non-unique physical response of C-band SAR to vegetation, soil moisture, surface roughness, and terrain geometry. Additional terrain and land-cover constraints are required before the output can be interpreted as a landslide map. (Handwerger et al., 2022; Mullissa et al., 2021; Phakdimek et al., 2023; Santangelo et al., 2022)

E-ISSN: 2948-5231
Journal of Asian Geography, 2026, Volume 5 (Issue 2), 46-58
https://doi.org/10.36777/jag2026.5.2.5

Consequently, the Batang Kali result is interpreted as a rapid disturbance-screening product that can prioritize locations for further inspection, not as a definitive landslide inventory. The Batang Kali case demonstrates both the operational value and the limitations of rapid SAR-based disturbance detection in a densely vegetated tropical mountain environment.

4.2 Lower Silesia Flood Case

The Lower Silesia analysis produced a complete Sentinel-2/ΔNDWI output for the AOI bounded by 16.85-17.45° E and 50.85-51.25° N. Four pre-event scenes from September 1-10, 2024, and three post-event scenes from September 16-25, 2024, were included in the archived workflow. The Δ*NDWI* layer contained coherent positive-change areas along portions of the river-floodplain corridor. These pixels were subsequently classified with the ΔNDWI ≥ 0.25 threshold. The spatial coherence of the signal is reported descriptively; its accuracy is assessed separately through the point sample (Figure 9).

The mapped pattern is consistent with water expansion after the September 2024 event, although Δ*NDWI* can also respond to wet soil, mixed pixels, atmospheric contamination, and land-cover change. The mapped patterns are also consistent with the broader context of the event described in the project materials, in which the 2024 flood in south-western Poland was linked to strong hydrometeorological factors and to flooding in riverine and lowland environments.

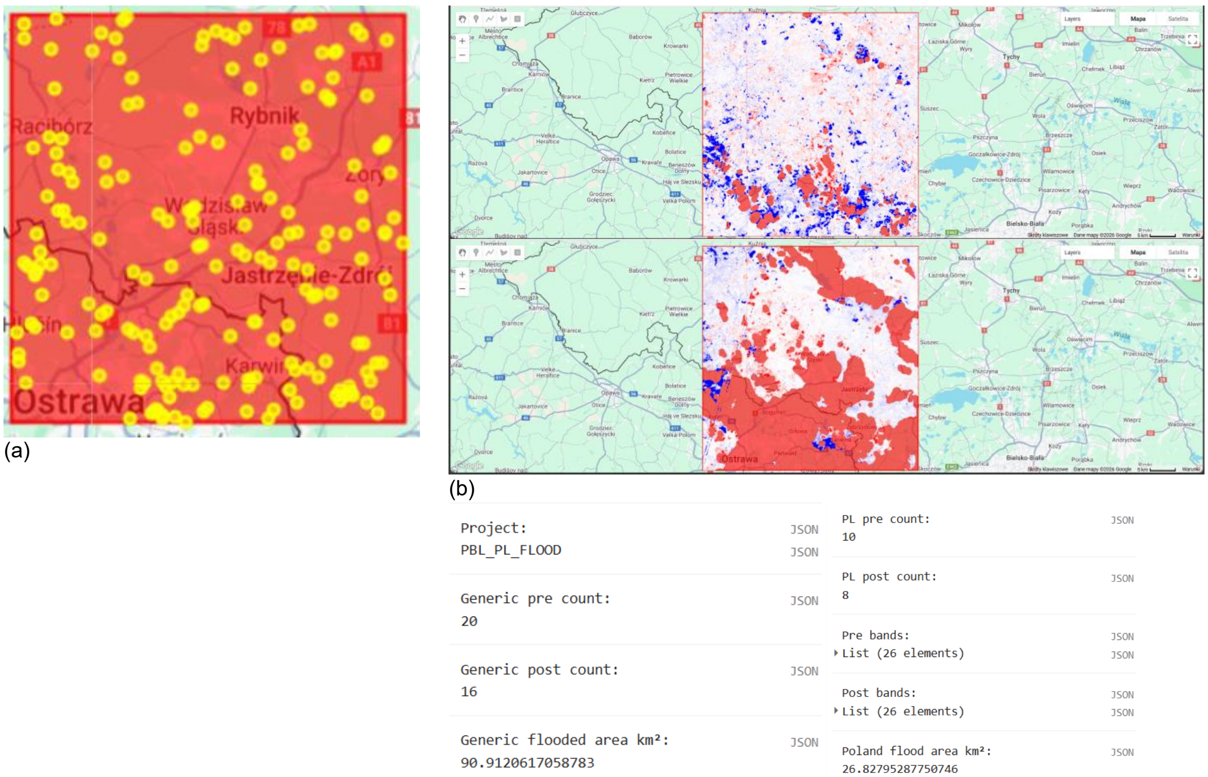

(a) (b) (c)

Figure 9: Analysis of the flooded areas in Poland (2024). Wodzisław Śląski city region: validation points, Δ*NDWI* generic + flood generic, Δ*NDWI* + flood (a) (b) and flooded areas (c).

Applying a threshold of ΔNDWI ≥ 0.25 produced 70.142 km² of flood-classified pixels within the analysed AOI. The mean and standard deviation of ΔNDWI were 0.0014716383 and 0.1463424363, respectively, and were used only to standardise the relative magnitude of change through the z-score transformation (Figures 9–11).

The flood branch therefore yielded both a binary flood-class mask and a standardised change-intensity surface. The standardised surface represents the relative magnitude of ΔNDWI change within the AOI and should not be interpreted as a direct measure of flood depth, hydraulic intensity, or flood risk.

The Lower Silesia internal validation sample contained 240 points, with 120 points sampled from each predicted class. The resulting confusion matrix contained 120 true positives (TP), 120 true negatives (TN), 0 false positives (FP), and 0 false negatives (FN), yielding 100% agreement in the validation sample for overall accuracy (OA), precision (user's accuracy), recall (producer's accuracy), specificity, F1-score, and balanced accuracy.

E-ISSN: 2948-5231
Article
Journal of Asian Geography, 2026, Volume 5 (Issue 2), 46-58
https://doi.org/10.36777/jag2026.5.2.5

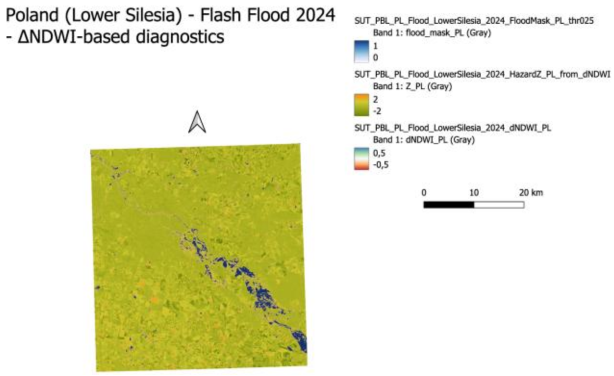

(a)

system:index	flood_mask_PL	Coordinates (longitude, latitude)	Reference Class
0	0	[17.060272439367587, 50.97652481103392]	NoWater
1	0	[17.0729732934399, 51.190977433091426]	NoWater
2	0	[17.428629344633958, 51.20445862555413]	NoWater
3	0	[16.957912628854892, 50.88664033618265]	NoWater
4	0	[17.047227073454348, 50.89041397084993]	NoWater
5	0	[17.03270796318224, 51.193123097206815]	NoWater
6	0	[16.8901235916899, 51.0102506096761]	NoWater
7	0	[17.41813077804284, 51.03666810821762]	NoWater
8	0	[16.950325337598454, 50.85816724965119]	NoWater
9	0	[17.306482690857198, 51.163851070680245]	NoWater
10	0	[17.010981550827477, 50.86433258076007]	NoWater
229	1	[17.28440813507524, 51.00644200639873]	Water
230	1	[17.44782702515509, 50.893580665228534]	Water
231	1	[17.25954345416808, 51.18095628815433]	Water
232	1	[17.32928685532243, 50.97461594936074]	Water
233	1	[17.426368737047717, 50.8911506995926]	Water
234	1	[17.20924386406294, 51.005639610462595]	Water
235	1	[16.998997980870318, 50.89979418817183]	Water
236	1	[16.888822725054332, 51.22701135991837]	Water
237	1	[17.208321037187687, 51.046219329794376]	Water
238	1	[16.86217169771848, 51.00287524816251]	Water

(b)

Figure 10: An example of Δ*NDWI* calculations for Lower Silesia along the Brzeg Dolny - Oława - Wrocław - Brzeg section (a), and an example of the classification as ‘NoWater’ and ‘Water’ for geographical coordinates (b).

This unusually high level of agreement should be interpreted cautiously. Candidate points were stratified based on the classified output, and reference classes were assigned through manual image interpretation. The project archive does not provide evidence of a fully independent, field-based reference dataset, and the same satellite imagery domain supported both the mapping and visual reference interpretation. The 100% result may therefore be optimistic and is reported as internal, image-based validation rather than independent confirmation of error-free flood classification (Foody, 2002).

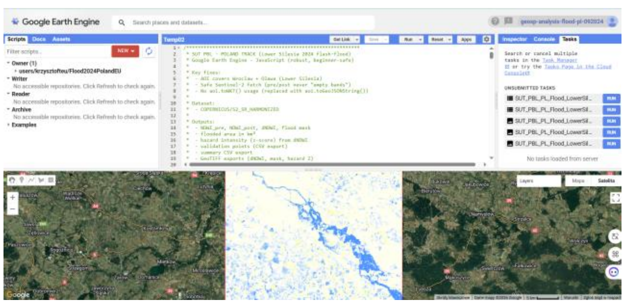

Project: SUT_PBL_PL_Flood_LowerSilesia_2024
Drive export folder: SUT_PBL_PL_Flood_LowerSilesia_2024
AOI GeoJSON string:
{"type":"Polygon","coordinates":[[[16.85,51.25],[16.85,50.85],[17.45,50.85],[17.45,51.25]]],"geodesic":false,"evenOdd":true}
PL pre window: 2024-09-01 to 2024-09-10
PL post window: 2024-09-16 to 2024-09-25
PL PRE - S2 count: 4
PL POST - S2 count: 3
PL PRE band names: ["B2","B3","B4","B8","QA60"]
PL POST band names: ["B2","B3","B4","B8","QA60"]
Poland flood 2024 - flooded area [km²] (ΔNDWI >= 0.25): 70.1420100106964
ΔNDWI mean over AOI (PL): 0.001471638317986427
ΔNDWI stdDev over AOI (PL): 0.1463424362703919

Figure 11: An example of Δ*NDWI* calculations for Lower Silesia along the Brzeg - Oława - Wrocław cities section in the GEE, showing the areas at risk of flooding (marked in blue).

Within these limitations, the flood branch demonstrates that the GEE workflow can produce a coherent flood-class map from openly available Sentinel-2 data using transparent processing and reproducible export procedures.

The results support the use of GEE for rapid flood screening without proprietary processing software, while highlighting the need for independent reference data when making quantitative accuracy claims. In practice, GEE can support rapid flood assessment without requiring proprietary or paid software, extensive local computing resources, or complex post-processing.

The workflow remained computationally simple and reproducible, making it suitable for technical training and rapid disaster risk reduction (DRR) applications. However, the present single-event result should not be generalised beyond the tested AOI without additional validation. The practical value of the flood branch therefore lies primarily in its accessibility, transparency, and reproducibility, rather than in a claim of universally high classification accuracy.

4.3 Comparative Result

In summary, both case studies demonstrate that the same GEE-based processing workflow can be successfully applied across two different hazard classes. However, its ultimate effectiveness depends on the physical characteristics of the selected indicator. For Lower Silesia (2024), the optical workflow produced coherent flood-related change patterns, with 100% agreement in the internal image-based validation sample. For Batang Kali (2022), the radar workflow was sensitive to surface disturbance but showed limited selectivity as a binary classifier. This contrast is central to the comparative interpretation. Workflow portability therefore does not imply equivalent classification performance. Google Earth Engine provided a single, stable computational architecture, but the final diagnostic behaviour remained specific to the hazard and physical indicator under investigation.

5.0 Discussion

The results should be interpreted at two interrelated levels. The first concerns the empirical patterns observed for the two hazards, while the second concerns the performance of a standardised and repeatable workflow implemented in Google Earth Engine and supported by freely available tools. The study was designed to assess methodological transferability rather than to imply equivalent hazard physics or universal classification performance. Although the common GEE architecture was successfully applied to both cases, the results demonstrate that workflow transferability and classification performance must be evaluated separately.

Both case studies, including the workflow variants developed during processing, followed the same general sequence: scene selection, change detection, generation of a threshold-based event mask, standardisation of relative change intensity, validation, and export. Google Earth Engine facilitated this consistency by providing a single computational environment for both the optical and radar branches of the analysis.

The Lower Silesia branch benefited from a relatively direct relationship between the physical process and the selected spectral indicator. An increase in surface water generally increases NDWI because water exhibits strong absorption in the near-infrared region. The

240-point validation sample showed complete agreement; however, this level of agreement is higher than would typically be expected from an independent validation exercise and should therefore be interpreted as an internal, image-based validation result. Previous GEE-based flood studies have highlighted the importance of independent reference data, threshold evaluation, and environmental context when assessing classification performance (DeVries et al., 2020; Nghia et al., 2022; Phakdimek et al., 2023; Singh & Rawat, 2024).

The flood result is therefore specific to the tested case and workflow. Dense vegetation, narrow water channels, urban shadows, wet soils, residual cloud contamination, and differences in image acquisition timing can reduce the separability of ΔNDWI. Furthermore, the present analysis does not include a preserved threshold-sensitivity analysis. Consequently, the selected threshold of 0.25 should not be interpreted as a generally optimal value. Its utility is demonstrated within the present workflow and AOI, but its broader applicability requires additional testing and independent validation.

The Batang Kali case presents a more challenging classification problem. Sentinel-1 is operationally valuable in tropical Asia because radar observations can be acquired under cloudy conditions and during both day and night. However, C-band backscatter is simultaneously influenced by surface moisture, vegetation structure, surface roughness, local incidence angle, and terrain geometry. Dense tropical vegetation and monsoon-related changes in surface moisture can therefore produce radar anomalies that are not uniquely associated with landsliding (Handwerger et al., 2022; Mullissa et al., 2021; Phakdimek et al., 2023; Santangelo et al., 2022).

The Batang Kali confusion matrix quantifies this limitation. Recall (producer's accuracy) was 100%, whereas precision was 9.17%, specificity was 0%, F1-score was 16.79%, and balanced accuracy was 50%. The method detected all 11 reference landslide points but classified all 109 stable reference points as landslide-like disturbances. The result therefore indicates high sensitivity but very limited discrimination between landslide-related and non-landslide-related radar changes. Accordingly, the workflow is better interpreted as a screening approach than as an inventory-grade landslide classifier. Recent landslide studies in Asia have improved discrimination by incorporating multi-temporal information, complementary optical and SAR indicators, terrain constraints, and explicit controls on false-positive detections (Phakdimek et al., 2023; Yang et al., 2024).

The comparison therefore supports a central methodological conclusion: a common computational workflow can be transferred across different hazards, but the physical indicator, threshold, validation design, and decision rules must remain hazard-specific. ΔNDWI and $\Delta\sigma^{o}$ are comparable as measures of relative change within a common analytical architecture, but they are not physically interchangeable measures of hazard intensity.

The two study areas also differ substantially in climate, land cover, relief, and process mechanics. Lower Silesia represents a temperate river and floodplain environment, whereas Batang Kali represents a densely vegetated tropical hillslope affected by monsoon rainfall and complex terrain. The study therefore does not establish universal performance from a single flood event and a single landslide event. Rather, it demonstrates the transferability of the computational architecture under two contrasting environmental and hazard conditions.

For future landslide applications, the $\Delta\sigma^{o*}$ approach could be strengthened by incorporating terrain variables such as slope, aspect, and elevation, together with drainage proximity, land cover, object- or cluster-based filtering, and multi-temporal SAR consistency. These additions should be evaluated empirically to determine whether they improve discrimination and reduce false-positive detections while retaining the screening sensitivity observed at Batang Kali. Previous studies suggest that terrain constraints, multi-temporal evidence, and complementary optical or SAR variables can improve false-positive control in GEE-based landslide detection (Handwerger et al., 2022; Mullissa et al., 2021; Phakdimek et al., 2023; Yang et al., 2024).

The broader contribution of the study is therefore methodological and operational. The PBL setting provided the framework within which the workflow was developed, but the scientific contribution lies in demonstrating that a single open, script-based GEE architecture can support two distinct post-event diagnostic tasks. For Malaysia and tropical Asia, the Batang Kali case further demonstrates the feasibility of rapid radar-based screening under cloud-prone conditions, while highlighting the importance of incorporating terrain and land-cover constraints before such approaches are applied to operational landslide mapping.

6.0 Conclusions

Overall, the study demonstrates that a standardised GEE-centred workflow can be transferred across flood and landslide case studies while preserving sensor-specific change metrics and a common sequence of preprocessing, change detection, classification, validation, and export. The Lower Silesia Sentinel-2/ΔNDWI branch produced coherent flood-related change and complete agreement in the internal point-based validation sample; however, because the reference interpretation was image-based rather than derived from an independent field inventory, this result should be regarded as case-specific and potentially optimistic. In contrast, the Batang Kali Sentinel-1/$\Delta\sigma^{o*}$ branch detected all reference landslide points but generated extensive false positives, indicating that its appropriate application is rapid disturbance screening and prioritisation for further verification rather than stand-alone landslide inventory, susceptibility, hazard, or risk mapping. These findings demonstrate that methodological equivalence does not imply identical diagnostic performance. Although ΔNDWI and $\Delta\sigma^{o*}$ can occupy parallel positions within a common analytical workflow, their physical meanings, uncertainties, thresholds, and validation requirements remain hazard-specific. For landslide applications, an important methodological refinement is therefore the integration of terrain characteristics, land cover, spatial-cluster logic, and multi-temporal SAR evidence to improve discrimination and reduce commission error. The principal contribution of the study is methodological: Google Earth Engine provides an accessible and reproducible computational architecture for rapid post-event geospatial diagnostics using openly available Sentinel data. The findings support further testing across additional events and independently validated datasets, particularly in tropical Asian environments where rapid, cloud-independent post-event assessment is operationally valuable.

Acknowledgement: This article presents excerpts from analyses carried out as part of the international PBL project between the Silesian University of Technology (Poland, EU) and Universiti Utara Malaysia (Malaysia), under the Silesian University of Technology - Excellence Initiative, during the winter semester of the 2025/2026 academic year (item 18 in the references).

Conflicts of Interest: The authors declare that there are no conflicts of interest in this study.

Data Availability Statement: The Sentinel-1 and Sentinel-2 source data are publicly available through the Copernicus program and Google Earth Engine. Derived rasters, validation tables, and project documentation used in this study are retained in the Silesian University of Technology-Universiti Utara Malaysia PBL project archive and are available from the corresponding author on reasonable request.

Author Contributions: Conceptualisation, methodology, investigation, data curation, formal analysis, visualisation, and writing – original draft preparation were contributed by the relevant members of the research team. Writing – review and editing, supervision, and project administration

E-ISSN: 2948-5231

Journal of Asian Geography, 2026, Volume 5 (Issue 2), 46-58
https://doi.org/10.36777/jag2026.5.2.5

were undertaken by the senior members of the research team. All authors contributed to the interpretation of the results, critically reviewed the manuscript, and approved the final version

Code Availability Statement: The Google Earth Engine workflow code used to carry out the analyses is stored in the PBL project archive and is protected as the authors' scientific output, as are the precise Sentinel-1 scene identifiers and the run-specific processing parameters from the original GEE project history.

Funding: This work was conducted within the international PBL project between the Silesian University of Technology and Universiti Utara Malaysia under the Silesian University of Technology Excellence Initiative during the winter semester of the 2025/2026 academic year.

References

Associated Press. (2023, October 18). Malaysia says landslide that killed 31 people last year was caused by heavy rain, not human activity. AP News. https://apnews.com/article/malaysia-landslide-natural-disaster-rainfall-86e2600fa8a57d761eaa06cf2dfd3c20

BK official report. Retrieved January 3, 2026, from https://batangkali31.com/bk-report/

Copernicus Data Space Ecosystem. Copernicus Browser. Retrieved February 14, 2026, from https://browser.dataspace.copernicus.eu/

DeVries, B., Huang, C., Armston, J., Huang, W., Jones, J. W., & Lang, M. W. (2020). Rapid and robust monitoring of flood events using Sentinel-1 and Landsat data on the Google Earth Engine. Remote Sensing of Environment, 240, 111664. https://doi.org/10.1016/j.rse.2020.111664

ECMWF. (2024, October 23). Storm Boris and European flooding, September 2024. https://www.ecmwf.int/en/about/media-centre/focus/2024/storm-boris-and-european-flooding-september-2024

European Space Agency. Sentinel-2. Retrieved January 4, 2025, from https://www.esa.int/Applications/Observing_the_Earth/Copernicus/Sentinel-2

Foody, G. M. (2002). Status of land cover classification accuracy assessment. Remote Sensing of Environment, 80(1), 185-201. https://doi.org/10.1016/S0034-4257(01)00295-4

Google. Google Maps. Retrieved February 14, 2026, from https://www.google.com/maps

Google Earth Engine. Google Earth Engine platform. Retrieved January 4, 2026, from https://earthengine.google.com/

Google for Developers. Google Earth Engine documentation. Retrieved January 3, 2026, from https://developers.google.com/earth-engine

Google for Developers. Harmonized Sentinel-2 MSI: MultiSpectral Instrument, Level-2A (SR). Earth Engine Data Catalog. Retrieved February 14, 2026, from https://developers.google.com/earth-engine/datasets/catalog/COPERNICUS_S2_SR_HARMONIZED

Google for Developers. Sentinel-1 SAR GRD: C-band Synthetic Aperture Radar Ground Range Detected, log scaling. Earth Engine Data Catalog. Retrieved February 14, 2026, from https://developers.google.com/earth-engine/datasets/catalog/COPERNICUS_S1_GRD

Gorelick, N., Hancher, M., Dixon, M., Ilyushchenko, S., Thau, D., & Moore, R. (2017). Google Earth Engine: Planetary-scale geospatial analysis for everyone. Remote Sensing of Environment, 202, 18-27. https://doi.org/10.1016/j.rse.2017.06.031

Handwerger, A. L., Huang, M.-H., Jones, S. Y., Amatya, P., Kerner, H. R., & Kirschbaum, D. B. (2022). Generating landslide density heatmaps for rapid detection using open-access satellite radar data in Google Earth Engine. Natural Hazards and Earth System Sciences, 22, 753-773. https://doi.org/10.5194/nhess-22-753-2022

Ibrahim, I. L., Hashim, N., Othman, A. N., Talib, N., & Shaharuddin, S. (2025). Landslide susceptibility assessment using Analytical Hierarchy Process (AHP) in Hulu Selangor. Revue Internationale de Géomatique, 34, 915-937. https://doi.org/10.32604/rig.2025.072321

Lower Silesian Voivodeship. Development strategy and regional characteristics of Lower Silesia. Retrieved February 2, 2026, from https://umwd.dolnyslask.pl/fileadmin/user_upload/_temp_/zalacznik_en.pdf

Majlis Perbandaran Hulu Selangor. (2023). Hulu Selangor Voluntary Local Review 2023. https://sdglocalization.org/sites/default/files/2025-06/Hulu%20Selangor%202023%20-%20EN.pdf

McFeeters, S. K. (1996). The use of the Normalized Difference Water Index (NDWI) in the delineation of open water features. International Journal of Remote Sensing, 17(7), 1425-1432. https://doi.org/10.1080/01431169608948714

Mullissa, A., Vollrath, A., Odongo-Braun, C., Slagter, B., Balling, J., Gou, Y., Gorelick, N., & Reiche, J. (2021). Sentinel-1 SAR Backscatter Analysis Ready Data Preparation in Google Earth Engine. Remote Sensing, 13(10), 1954. https://doi.org/10.3390/rs13101954

NASA. Worldview. Retrieved January 3, 2026, from https://worldview.earthdata.nasa.gov/

Nasze Miasto. (2024). Wielka Woda 2024 in the Silesian Voivodeship: Wodzisław Śląski flood documentation. https://wodzislawslaski.naszemiasto.pl/tu-rozegral-sie-dramat-wielka-woda-2024-w-woj-slaskim/ar/c1-9798507

Nghia, B. P. Q., Pal, I., Chollacoop, N., & Mukhopadhyay, A. (2022). Applying Google Earth Engine for flood mapping and monitoring in the downstream provinces of Mekong River. Progress in Disaster Science, 14, 100235. https://doi.org/10.1016/j.pdisas.2022.100235

Phakdimek, S., Komori, D., & Chaithong, T. (2023). Combination of optical images and SAR images for detecting landslide scars, using a classification and regression tree. International Journal of Remote Sensing, 44(11), 3572-3606. https://doi.org/10.1080/01431161.2023.2224096

QGIS.org. (2026). QGIS Geographic Information System. QGIS Association. https://qgis.org

Santangelo, M., Cardinali, M., Bucci, F., Fiorucci, F., & Mondini, A. C. (2022). Exploring event landslide mapping using Sentinel-1 SAR backscatter products. Geomorphology, 397, 108021. https://doi.org/10.1016/j.geomorph.2021.108021

Singh, A. (1989). Digital change detection techniques using remotely-sensed data. International Journal of Remote Sensing, 10(6), 989-1003. https://doi.org/10.1080/01431168908903939

Singh, G., & Rawat, K. S. (2024). Mapping flooded areas utilizing Google Earth Engine and open SAR data: A comprehensive approach for disaster response. Discover Geoscience, 2, 5. https://doi.org/10.1007/s44288-024-00006-4

Tomiczek, K. M. (head supervisor) et al. (2026). Geospatial data analysis in diagnostic applications for disaster land management (unpublished PBL project report). Silesian University of Technology-Universiti Utara Malaysia.

Yang, Y.-E., Yu, T.-T., & Chen, C.-Y. (2024). Automatic detection of landslide impact areas using Google Earth Engine. Terrestrial, Atmospheric and Oceanic Sciences, 35, 17. https://doi.org/10.1007/s44195-024-00078-2